REPORT
doi:10.26443/seismica.v5i2.2818

SEISMICA

A catalogue of 5000 aseismic slip events from the San Andreas, Anatolian, Dead Sea and Chaman fault systems

Daniel B. Gittins * [1,2], **Kathryn Materna** [1,2], **Heather Crume** [3], **Najeebullah Kakar** [4], **Yariv Hamiel** [5], **John Langbein** [6], **Roger Bilham** [1,2]

[1]CIRES, University of Colorado Boulder, Boulder, USA, [2]Department of Geological Sciences, University of Colorado Boulder, Boulder, USA, [3]Santa Cruz Geophysics, Inc., Santa Cruz, USA, [4]Department of Geology, University of Balochistan, Balochistan, Pakistan, [5]Geological Survey of Israel, Jerusalem, Israel, [6]U.S. Geological Survey, Moffett Field, USA

Author contributions: *Conceptualization*: Daniel Gittins, Kathryn Materna, Roger Bilham. *Data collection*: John Langbein, Roger Bilham, Heather Crume, Yariv Hamiel, Najeebullah Kakar. *Software*: Daniel B Gittins. *Formal Analysis*: Daniel B Gittins. *Writing - Original draft*: Daniel B Gittins. *Writing - Review & Editing*: Daniel B Gittins, Kathryn Materna, Roger Bilham, Heather Crume, John Langbein, Yariv Hamiel, Najeebullah Kakar. *Visualization*: Daniel Gittins. *Funding acquisition*: Daniel Gittins.

Abstract Steady aseismic slip on surface faults (creep) is occasionally interrupted by an impulsive or emergent acceleration in slip that offsets a surface fault by a few millimetres over a period of several hours to many days. We present here a catalogue of 5695 episodic events recorded by 78 creepmeters on creeping faults worldwide between 1980 and 2023. The events vary in amplitude from < 1 millimetre to > 1 centimetre, have durations from a few hours to a few weeks, and have been recorded on creepmeters at sampling rates from 1 second to 1 hour. Typical instrument resolutions are several microns. This work presents the overall features of these 5000+ events, evaluates patterns of their occurrence through space and time, and provides the resulting catalogue in a unified form to facilitate future investigations.

Non-technical summary Slip on most tectonically active faults occurs in earthquakes; however, some faults have been observed also to slip steadily on the surface at a rate too slow to be perceived with the naked eye, by a process known as fault creep. A subset of these creeping faults shows an intermediate form of slip in which slow steady slip is interrupted by intervals of brief acceleration, causing the surface fault to slip by a few millimetres in hours or days. We have identified more than 5000 of these transient episodes of slip and provide a catalogue of them in digital form suitable for easy access. The data provide the precise time history of each slip event and will form a data base for those interested in analysing the role of creep events in reducing seismic hazards.

Production Editor:
Gareth Funning
Handling Editor:
Meng Wei
Copy & Layout Editor:
Théa Ragon

Received:
March 13, 2025
Accepted:
August 17, 2026
Published:
September 11, 2026

1 Introduction

Aseismic slip was first observed on the San Andreas fault in central California in 1955 (Steinbrugge et al., 1960). Even in these early data it was recognized that slow steady surface creep was occasionally interrupted by accelerations in slip characterized by an abrupt increase in velocity from μm/day to μm/s, which subsequently slowed with time to pre-event velocities. These transient events generally produced a few mm to cm of fault slip over hours or days, and together accounted for much of the annual surface slip of the fault. They were initially called "spasms" and have recently been described as surges in slip (Gittins and Hawthorne, 2022) but are more generally known as episodic creep events (ECEs). Episodic creep events have now been observed on numerous faults, both at the surface recorded by creepmeters (e.g., Hamiel et al., 2025; Schulz, 1989; Tocher, 1969; Yamashita and Burford, 1973), and on faults at depth recorded by strainmeters or inferred geodetically (Evans et al., 1981; Gittins and Hawthorne, 2024; Goulty and Gilman, 1978; Hamiel and Piatibratova, 2023; Materna et al., 2024; Tymofyeyeva et al., 2019; Vavra et al., 2024). They are now recognized to contribute to a broader spectrum of fault failure from slow slip to earthquakes (Bürgmann, 2018; Peng and Gomberg, 2010; Sacks et al., 1982). Because surface creep events offer a spatial scale of slip instability intermediate between that of laboratory experiments of incipient nucleation (<1 m) and damaging earthquakes (>10 km), their study provides potential insights into the mechanisms leading to and following failure of active faults.

An important tool for the measurement of aseismic slip and its temporal variations comes from instruments called creepmeters. These devices measure the extension of a ~10-meter baseline installed across the trace of a fault (Bilham et al., 2004), and their data are valuable indicators of fault slip because of their extremely high precision (i.e., tens of μm) and high temporal resolution (i.e., seconds or minutes) compared to other

*Corresponding author: tees.seis96@gmail.com

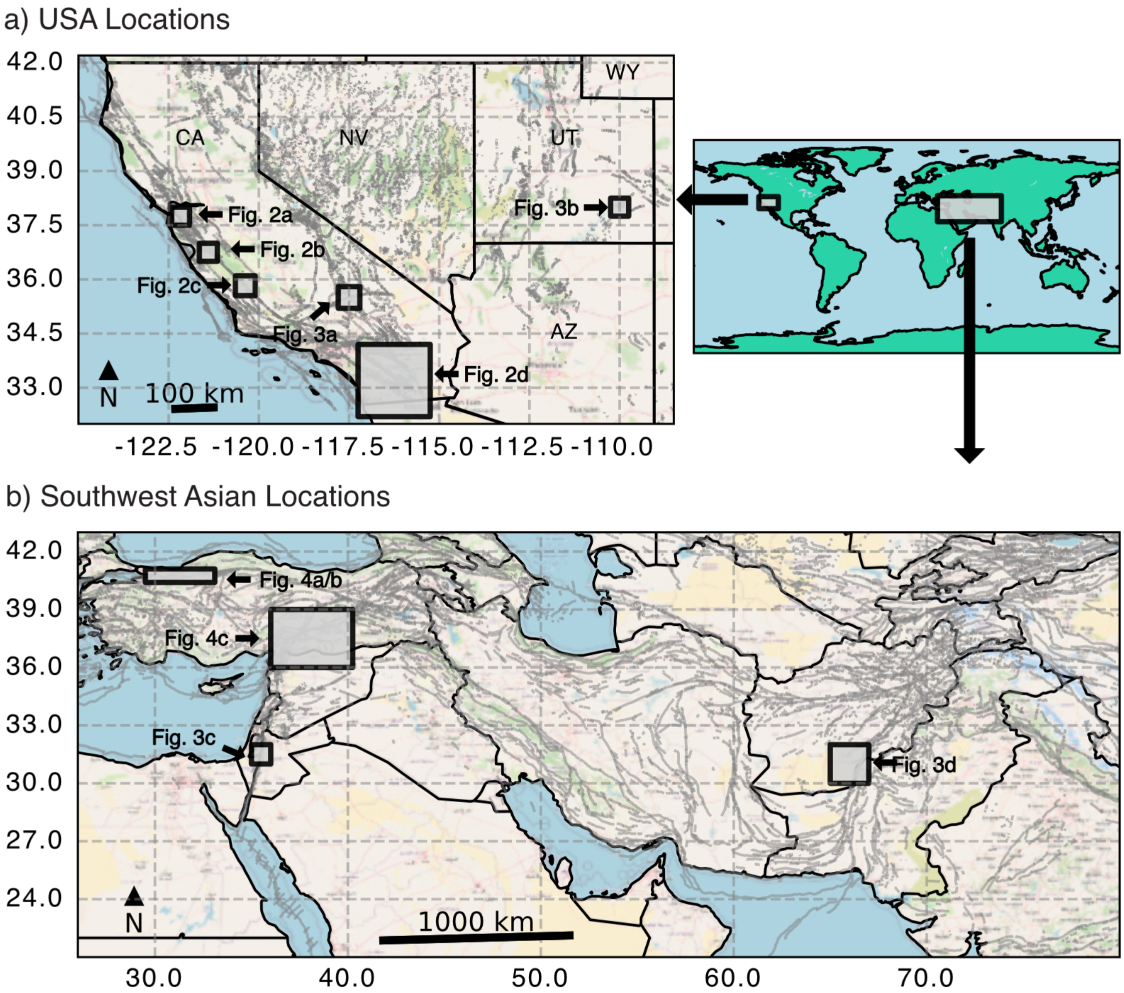

Figure 1 Map of creepmeter locations shown in Figure 2 – 4 for a) USA locations and b) Southwest Asian locations. Faults from the Quaternary Fault and Fold Database (USGS and CGS, 2020) are shown as grey lines in panel a). Faults from Zelenin et al. (2022) are shown as grey lines in panel b).

geodetic methods (Langbein et al., 2024; Schulz et al., 1982). Creepmeter installations are sometimes motivated by observations of interseismic creep and sometimes with the purpose of capturing earthquake afterslip (Langbein et al., 2024), but in either case, creepmeters are generally installed on faults that are highly localized when they reach the surface. As a result, most creepmeter measurements generally come from continental strike-slip faults. On reverse and normal faults, creepmeters are more difficult to install successfully, as surface weathering often obscures the presence of creep and the expression of faulting in these systems may be more broadly distributed. On the many fault systems where creepmeters are now installed, they provide long-term observations of fault slip processes with high temporal resolution and measurement precision. However, while many creepmeter measurements are currently available in various ways, at present they are not fully analysed into a global description of fault slip.

In order to further our understanding of aseismic fault creep, we here develop the world's largest catalogue describing the time history of creep events from a compilation of creepmeter data. While these observations describe the deformation of the shallow fault zone, they also provide constraints on fault failure more broadly. We present these creep data and the associated creep event catalogue to advance the systematic study of episodic creep events. We then consider the implications of these data for the general rheology of fault zones and the nucleation of stick-slip failure processes.

2 Creepmeter dataset

We examine data from 78 creepmeters located on 16 creeping faults on four continents (Figure 1). The faults include the San Andreas, Hayward, Calaveras, Imperial, Superstition Hills Faults, minor faults in southernmost California, normal faults in Canyonlands, Utah (Figure 1a), the Dead Sea Fault system in Israel, the Chaman Fault in Pakistan, and the North and East Anatolian Faults in Türkiye (Figure 1b). We do not consider the orthogonal component of paired creepmeter installations which have been shown to alter the calculated fault parallel displacement recorded on creepmeters (Langbein et al., 2024) because paired creepmeters are only installed at a few locations and we wanted to ensure consistency of identification and processing across sites and regions for simplicity.

In California, we examine data from 51 creepmeter locations (some of which have multiple sensors) which are installed within five regions: the Hayward Fault (Figure 2a), the Calaveras and San Andreas Faults near San Juan Bautista (Figure 2b), and the San Andreas Fault near Parkfield (Figure 2c). In Southern California we examine data from the southern San Andreas Fault between Indio and Bombay Beach, from the Superstition Hills Fault and Imperial Fault (Figure 2d), an area we will refer to as the Salton Trough region. We also consider data from newly ruptured faults near Ridgecrest and from the Garlock Fault (Figure 3a). In Utah (Figure 3b), we examine data from one creepmeter installed across a normal fault in Canyonlands National Park (Kravitz et al., 2020). In Türkiye, we consider 24 creepmeters on the North (Figure 4a/b) and East Anatolian Faults (Figure 4c). In Israel (Figure 3c), we consider one creepmeter on an oblique normal/left-lateral fault within the Dead Sea Fault Zone. In Pakistan (Figure 3d), we consider one creepmeter on the Chaman Fault.

In all cases, we use all available creepmeter data between 2 February 1980 and 31 December 2023, amounting to 633 site-years of creepmeter time series. We did not include creepmeter data prior to 1980 as these were recorded on paper charts. Within the 1980-2023 dataset, different instruments naturally span various lengths of time and may have different sampling rates (see Tables S1-S7 for details). The highest and lowest sampling rates within the dataset are 1 second and 60 minutes, respectively. By far the longest record of creep comes from central California, recorded by the U.S. Geological Survey with typical sampling rates of 10 minutes.

3 Manual Detection of Slip Events

To develop the catalogue in the present work, we first developed our creep event detection criteria based on prior work. We considered but ultimately did not adopt the creep event detection technique of Gittins and Hawthorne (2022), which used cross-correlation to detect creep events from the central San Andreas Fault. The Gittins and Hawthorne (2022) catalogue identified > 2000 creep events, but the method omitted a number of creep events with especially abrupt onsets, small amplitudes, low peak velocity, or long slip duration, and failed to separate the timing of individual events within longer, multi-event sequences. Furthermore, the most significant drawback of the cross-correlation technique was that a large number of false-events were detected: only 14% of potential slip accelerations in the catalogue were actual events (Gittins and Hawthorne, 2022). Most of these false-events were stick-slip events caused by the internal friction within the creepmeter, which manifest as abrupt offsets between two contiguous data points within the creepmeter data that are not associated with the timing of nearby or teleseismic earthquakes.

We also examined the creep event detection method of Langbein et al. (2024), which was designed to estimate the ratio between steady creep and episodic creep, but ultimately decided against using it in the present work. This method was designed only to identify events with slip rates exceeding the long-term slip rate by a factor of 10. In contrast, our goal was to identify a wide spectrum of creep acceleration processes. It is likely therefore that there will be a difference in identified events between the catalogue presented here and Langbein et al. (2024). In further analysis of events it is advised therefore to assess this catalogue in tandem with other catalogues of events (e.g., Langbein et al., 2024).

To avoid these errors and biases in the current catalogue, we chose to identify creep events manually in the records from 78 creepmeters available globally. We chose manual identification as this allowed us to isolate creep accelerations while accounting for the unique data features of each creepmeter time series, such as variable sampling rates or noisy data periods. For data from the 18 creepmeters along the central San Andreas Fault, we used the start times identified by Gittins and Hawthorne (2022) as an initial guide for identifying creep events, but also identified additional events missed by that technique.

Then, we examined three-month long data windows and picked an approximate start time for individual events by zooming into the time series. The three month window was chosen as a compromise between accuracy and efficiency, producing high-sensitivity detection while still permitting manual inspection through the entire dataset. Following this, we examined progressively longer time windows extending out to two to three years and identified a reasonable end time for each event in the window, which was defined as the time when the slip returned to a pre-event background rate or the time at which the ongoing event was interrupted by a new event. We justify the use of dual windows because creep events usually start impulsively, requiring short windows to identify their onset. Then, the slip slowly returns to its background rate, requiring a longer time window to identify the cessation of the event. We then examined the time series as a whole (i.e., the full 30 year timeseries if a creepmeter operated for 30 years) to identify any clear and obvious omitted events, most of which occurred at the start or end of the selected three-month windows. Finally, we quality checked each individual event, assigning a precise start and end time, splitting events into sequences of events if they appeared to contain distinct accelerations and removing any events that were originally identified but were deemed as noise on further more detailed examination.

One potential complication in event detection is the occurrence of multiple creep events in a sequence. Event sequences can often have 3–12 events that interfere constructively, meaning event X may not have fully completed before event Y begins and that event Y is made up of both event X and Y's displacements. In this catalogue, we have chosen to record the timing of all events separately, even if they form an event sequence; we consider it important to characterize the timing of each acceleration in the event sequence, as these accelerations may originate from asperities in different locations along the fault (Gittins and Hawthorne, 2024). However, event sequences do introduce uncertainty in the total displacement of each event within the multi-event time series. In such event sequences, fully disentangling individual events may require fitting a curve to the time series of each superimposed event simultane-

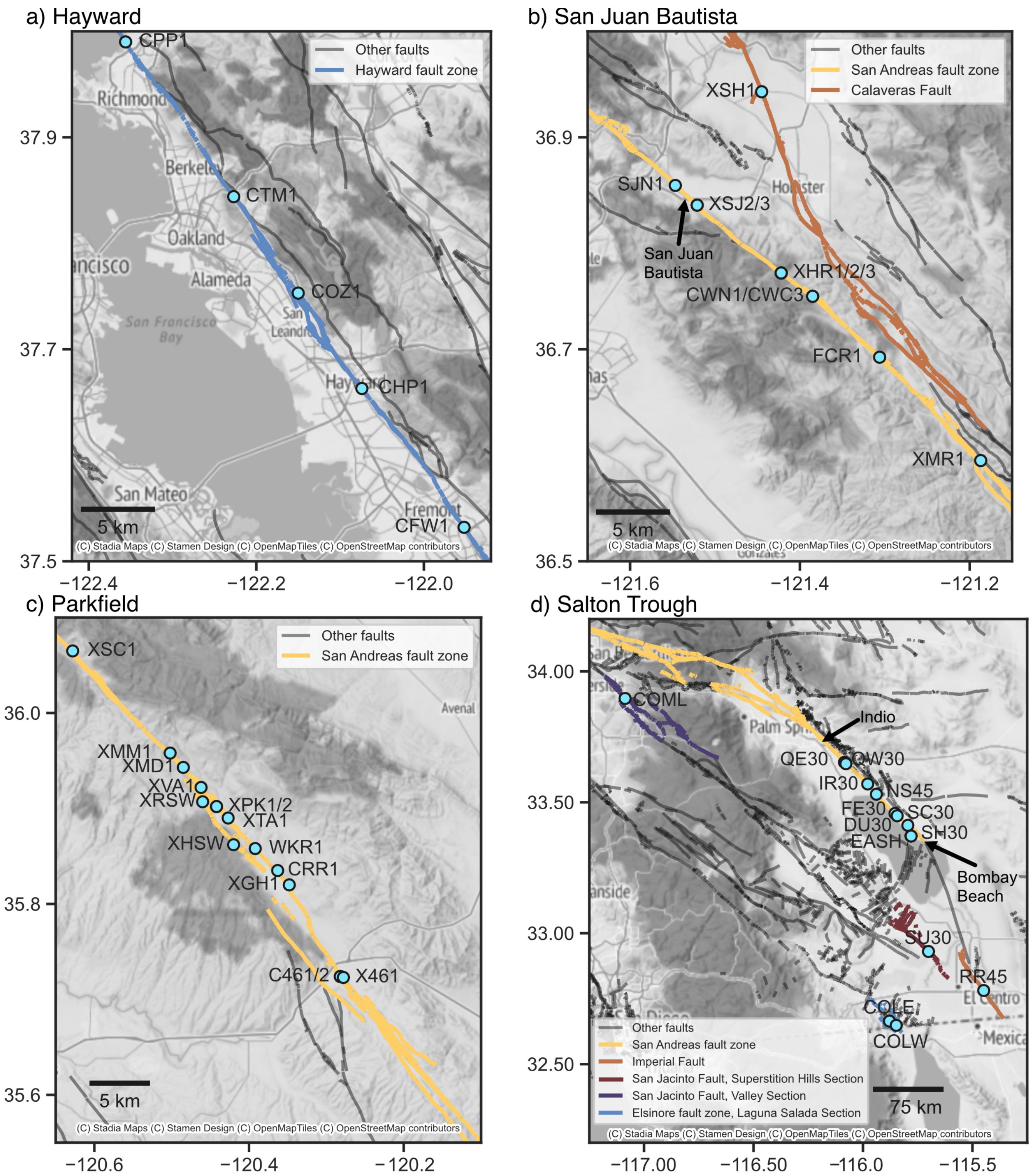

Figure 2 Maps of major creepmeter locations in California. a) Map of Hayward creepmeters. b) Map of San Juan Bautista creepmeters. c) Map of Parkfield creepmeters. d) Map of Salton Trough creepmeters. Faults are from the Quaternary Fault and Fold Database (USGS and CGS, 2020) are shown as grey lines with important faults highlighted. The grayscale colours represent topography.

ously. This type of functional fitting has been done for individual events in isolation (Gittins and Hawthorne, 2026), but is more complicated for events in multi-event sequences and is beyond the scope of this study.

Following the techniques described above, we identified 5695 transient accelerations in slip in the global dataset of 78 creepmeters, and we compiled these detections into an event catalogue. For each event identified in this study, the catalogue includes a unique identifier, start time, end time, duration and displacement. Each event is also labelled as belonging to one of the taxonomic groups of Section 4. Then, section 5 discusses the specific characteristics of events in each location and over time.

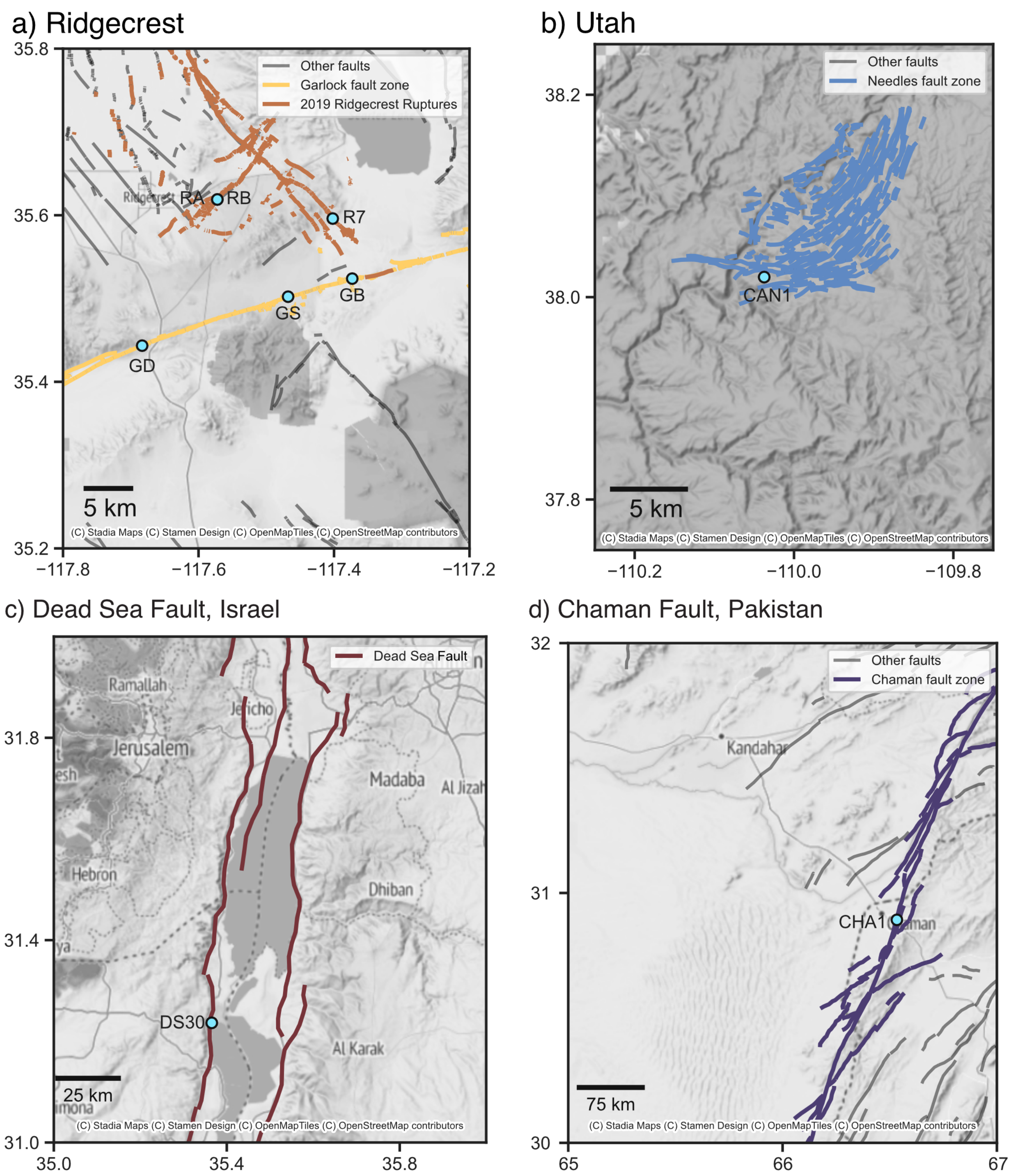

Figure 3 a) Map of Ridgecrest, California creepmeters. b) Map of Utah creepmeter. In a) & b) faults are from the Quaternary Fault and Fold Database (USGS and CGS, 2020) are shown as grey lines with important faults highlighted. In b) the 2019 Ridgecrest rupture extent is brown lines (Ponti et al., 2020) and extends off the map to the northwest. c) Map of creepmeter in Israel. d) Map of creepmeter in Pakistan. In c) & d) faults from Zelenin et al. (2022) are as grey lines with important faults highlighted in yellow.

4 Taxonomy of aseismic slip behaviours on creepmeters

Aseismic slip on faults forms a continuum of processes from seconds to years. However, six prominent modes of aseismic slip behaviour may readily be identified in the present catalogue: steady creep, episodic creep events, triggered slip, afterslip, a class of miniature creep events with small amplitude that we term creeplets and long-period creep accelerations. Former studies considering the taxonomy of aseismic surface slip (Schulz, 1989; Sylvester, 1986) have not included the last two of these modes of slip. While these six modes of slip are prominent in creepmeter time series and have

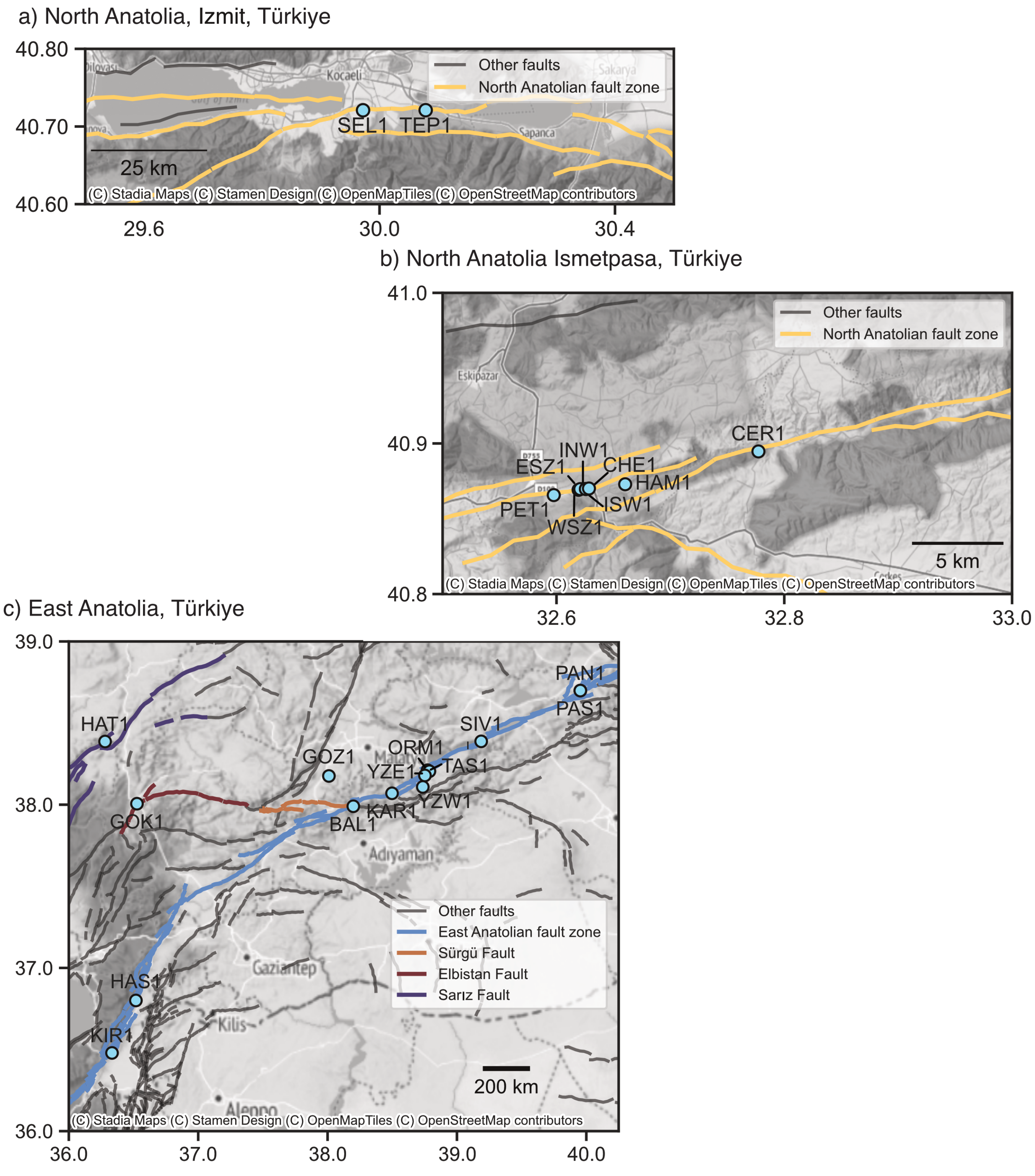

Figure 4 a) Map of creepmeters along the Izmit section of the North Anatolian Fault. b) Map of creepmeters along the Ismetpasa section of the North Anatolian Fault. c) Map of creepmeters in East Anatolia. Faults from Zelenin et al. (2022) are as grey lines with important faults highlighted.

common ways of presenting, we note that they are not entirely mutually exclusive. In this section, we first introduce these six prominent modes, and in later sections we discuss the hybrid modes that make up the spectrum of slow slip behaviours.

4.1 Steady Creep

Steady creep refers to fault displacement that accumulates linearly with time with no transient accelerations in slip. Figure 5a illustrates steady creep at Temescal along the Hayward fault (CTM1). Some fault slip time series are dominated by steady creep with few or no events (e.g., Point Pinole on the Hayward Fault, CPP1), while others show some degree of steady creep supplemented by other transient modes of slip (Langbein et al., 2024). At some locations, the observed creep velocities between slip events may be close to zero (e.g., Superstition Hills Fault, SU30), whereas at other locations (e.g., Slacks Canyon, XSC1) steady creep may exceed slip velocities of 21 mm/year (≈ 2 μm/hour) (Langbein et al., 2024).

4.2 Episodic Creep Events

Episodic creep events (ECEs) (Figure 5b) are abrupt accelerations in slip from steady creep (i.e., at velocities $\leq$1 μm/hour) to slip velocities that may exceed 1 μm/minute after a few minutes. Slip velocities subsequently decay over the next several hours or days as they asymptotically approach pre-event levels. ECEs are thought to represent a spontaneous failure process due to the release of a steadily increasing antisymmetric strain near the fault. ECEs are effectively slow earthquakes, although their equivalent moment-magnitudes can rarely be determined due to the absence of information concerning their along-strike slip or depth. Episodic creep events have been the focus of numerous studies for their potential to provide constraints on the rheology and/or geometry of shallow fault zones (Gittins and Hawthorne, 2022; King, 1972; Langbein et al., 2024; Nason et al., 1974; Schulz, 1989; Schulz et al., 1976; Wesson, 1988; Yamashita and Burford, 1973). Creep events observed on creepmeters are often preceded by an initial strain signal corresponding to the approach of a subsurface dislocation before the commencement of slip (King et al., 1977). The critical failure strain – the transition from shear strain to discrete slip of the surface fault – occurs when strain exceeds $\approx 10^{-5}$ ($\approx$100 μm in a 10 m long creepmeter). For the most readily identified creep events, the transition from strain to slip typically occurs within 5 minutes, in proportion to the propagation velocity and amplitude of the approaching dislocation. The maximum slip rates typically occur within the next two minutes as strain is released from the flanks of the fault. Slip velocities then reduce exponentially to pre-event rates over a few hours or days. Figure 5b shows an example of one of these events.

4.3 Triggered Slip

Triggered slip is defined here as slip on a fault that occurs during and immediately following the passage of surface waves propagating from a local or teleseismic earthquake (Allen et al., 1972). Dynamic creep triggering has been observed on creeping faults for decades and is especially common in some parts of the world, such as southern California (Williams et al., 1988; Hudnut and Clark, 1989; Bodin et al., 1994; Donnellan et al., 2014; Wei et al., 2015; Victor et al., 2018; Tymofyeyeva et al., 2019; Bilham and Castillo, 2020). We note that there is also some evidence that earthquake-generated static stress changes can affect creep rates (Lienkaemper et al., 1997; Xu et al., 2018), but this effect is harder to identify in time series alone and requires event-specific modelling, so here we focus on the potential effects of dynamically triggered slip in the identified creep events.

When recorded on a creepmeter, triggered slip often takes the form of a step-like offset of microns to millimeters (Bilham and Castillo, 2020; King et al., 1977). Where sampling rates are rapid ($\geq$ 1Hz), triggered slip is observed to be a progressive slip process with a duration of several seconds during exposure of the fault to dynamic strain. Triggered slip direction is usually in the sense of persistent fault slip (i.e. triggered slip is dextral on dextral faults); however, seasonal stress in the fault zone may occasionally result in triggered slip with opposite polarity to the long term slip of the fault. The offset may be complete within a few seconds, or slip may increase for several minutes after the triggered event, followed by an extended period of quiescence or reduced creep rate. The duration, t, of this subsequent creep quiescence depends on the amplitude of triggered slip, and the pre-event creep rate, c, such that $t \approx d/c$ (Bilham and Hough, 2024). Hence triggered slip appears to represent the recovery of a local shallow slip deficit on the fault during a reduction of friction or effective normal stress associated with transient dynamic strains applied to the fault zone.

Triggered slip was initially considered indistinguishable from instrument instability, especially in cases where the data were recorded at a low sampling rate (e.g., Figure 5c, 2010 M 7.2 El Mayor Cucapah earthquake recorded at 15 minute sampling on the Superstition Hills Fault). In such cases, triggered slip can be complete between two contiguous data samples. However, in recent cases where triggered slip has been recorded at rates of 1 second to 1 minute, it is clear that the fault zone responds to the transient oscillatory dynamic strain associated with the passage of seismic waves, and that slip is initiated on the fault during the passage of large-amplitude, long-period surface waves. Triggered slip amplitudes often do not exceed 1 mm, but in exceptional cases, triggered slip may be > 1 cm. On faults where episodic creep events also occur, it is common for surface waves to advance the timing of a pending event, and to thereby release slip exceeding several mm. In such instances slip may have a prolonged duration of days or months (e.g., Tymofyeyeva et al., 2019).

In this catalogue, we provide an empirical test for triggered slip induced by local earthquakes. For each event detected, we determined the potential correlation with M $\geq$3.0 earthquakes within 500 km based on the thresholds in Victor et al. (2018) to establish local triggering relationships. We require the triggered slip amplitude to be at least 5 μm, or 0.5 μstrain in a 10-m-long creepmeter, because smaller offsets are below the noise level of the creepmeter. We first identify a temporal search window of $R/3.0 \pm 5s$, where s is the sampling interval in seconds, R is the epicentral distance in km, and 3.0 km/s is an assumed typical surface wave velocity. We apply an empirical relationship from Barbour et al. (2021) to determine whether an earthquake of given Mw is anticipated to generate dynamic strain at the creepmeter equal to or exceeding 5x10^{-7} (Bilham and Hough, 2024). Events that satisfy these criteria are noted in the catalogue as possible triggering events. These criteria do not constitute an exhaustive test since they exclude, for example, M < 3 local events, large

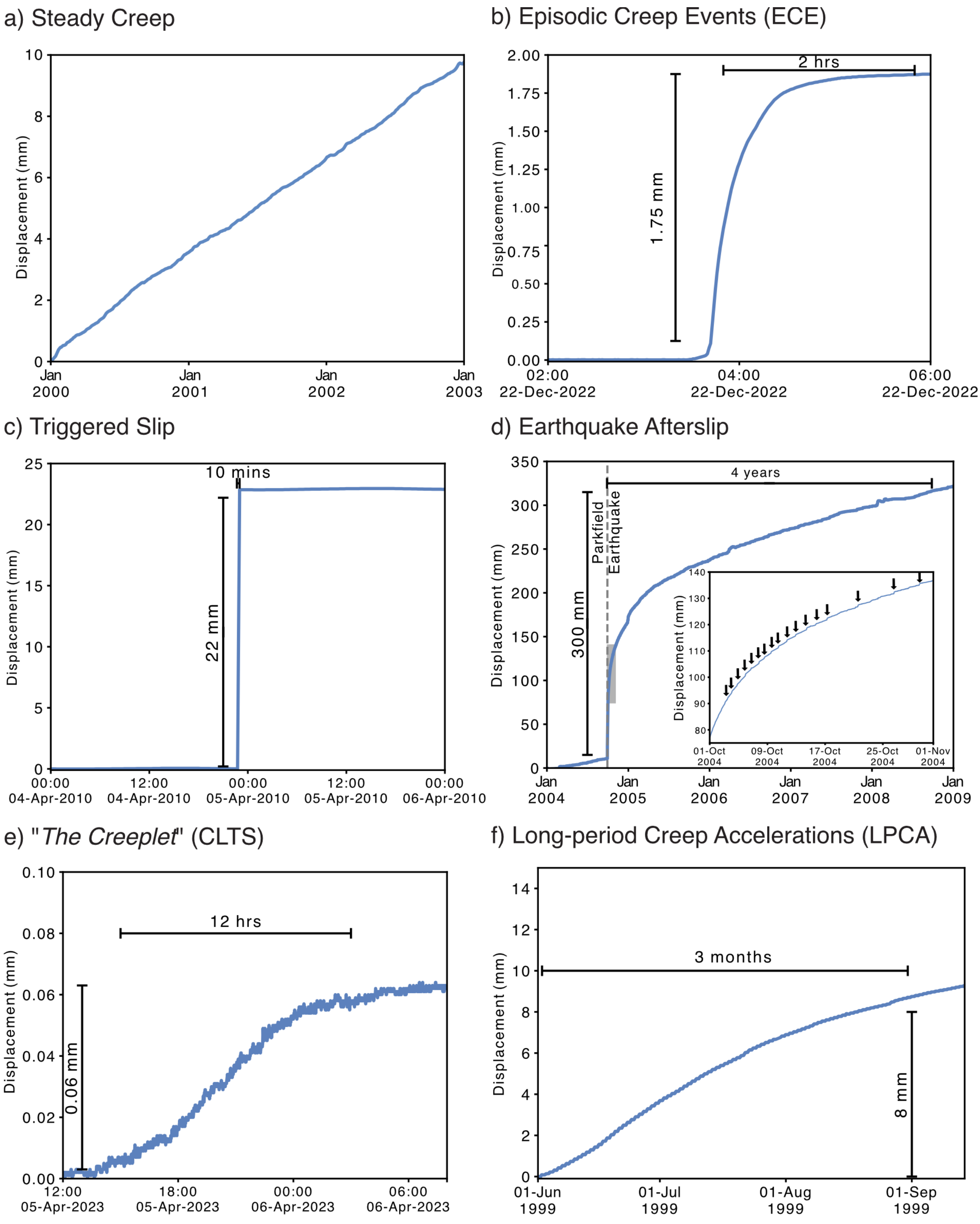

Figure 5 Examples of aseismic slip types. a) Steady creep (CTM1). b) Episodic creep event (XMR1). c) Triggered slip (SU30). d) Earthquake afterslip (XMM1), inset shows timing of episodic creep events on top of the afterslip signal. e) Creeplet (CWN1). f) Long-period Creep Acceleration (XVA1).

teleseismic events at distances > 500 km, or delayed triggering of slip on the fault near the creepmeter propagating from slip triggered at depth or along the fault.

Beyond earthquakes, creep events may also be induced by other types of environmental changes, but we do not indicate these potential triggers in the catalogue.

For example, creep events on the North Anatolian Fault in Ismetpasa have been triggered at times of low atmospheric pressure (R. Bilham, 2026, p.c.). Rainfall is also known to be closely correlated with the timing of creep events (Roeloffs, 2001; Schulz et al., 1983) and is a potential trigger of accelerated aseismic slip. However, as this effect is not yet well understood, we consider the triggering of creep by environmental mechanisms to be beyond the scope of the current catalogue.

4.4 Afterslip

Afterslip is a postseismic process whereby portions of the fault slip aseismically in response to stresses associated with coseismic slip at depth (Marone et al., 1991; Perfettini and Avouac, 2004). As observed on creepmeters, afterslip at the surface typically starts minutes to days after an earthquake (Ambraseys, 1970; Langbein et al., 2006; Bilham et al., 2025; Cakir et al., 2023; Bilham, 2005) and grows over subsequent months or years. The rate of afterslip typically takes the form of an impulsive acceleration in slip followed by a slip velocity which decays logarithmically with time. As a rule of thumb, as much surface slip occurs in the first week after the mainshock as occurs in the succeeding 10 weeks, as in the following 100 weeks etc. Afterslip has been documented on numerous faults: e.g., the San Andreas Fault at Parkfield (Freed, 2007; Johnson et al., 2006; Langbein et al., 2006; Savage and Langbein, 2008; Smith and Wyss, 1968), Superstition Hills Fault (Marone et al., 1991), East Anatolian Fault (Cakir et al., 2023), Motagua Fault in Guatemala (Bucknam, 1978), the Xianshuihe Fault in China (Tong and Chen, 2025), and North Anatolian Fault (Bilham et al., 2016).

Figure 5d shows an example of afterslip on the San Andreas Fault after the 2004 M6.0 Parkfield earthquake as recorded at Middle Mountain (XMM1). At long timescales this afterslip appears smooth; however, the slip process is often manifest on the surface as a sequence of episodic creep events separated by intervals that increase with the logarithm of elapsed time. (Figure 5d, inset).

4.5 Creeplets

We invoke the term "creeplet" (CLTS) (Figure 5e) to describe a class of fault-slip event with amplitude 20-100 μm, close to the instrumental noise level, and duration >5 minutes. These events are abundant in creep records, and many have hitherto been dismissed as environmental noise, or artifacts of instrument operation ("stiction" or monument instability). The difference between creeplets and stiction artifacts is shown in Figure S1. We arbitrarily define the minimum amplitude of creeplets as 20 μm, and with a duration of at least 5 minutes (five times longer than the sampling interval of 1-minute sampled data). Creeplets may occur as a smoothed step (Figure 5e) or may nucleate abruptly and decay slowly, with a time history similar to episodic creep events, but are distinguished by their shorter duration and smaller amplitude. As with triggered slip, their small amplitudes have historically rendered creeplets difficult to distinguish from artifacts in the instrument, particularly in the more recent extended-range creepmeters that incorporate several moving parts (Langbein et al., 2024). It is probable that some of the offsets identified as creeplets are indeed instrumental artifacts; however, their presence in records obtained from the friction-free catenary wire creepmeters of Yamashita and Burford (1973) indicates that they cannot be entirely dismissed as instrumental noise.

4.6 Long-period Creep Accelerations

Long-period Creep Accelerations (LPCAs) are increases and decreases in surface slip rate with durations of weeks to < 6 months. In these surges, slip accelerates slowly from background velocities and decelerates subsequently to former levels over the course of several months (Figure 5f). Due to their slow emergent onset, the rate changes are less pronounced than that of episodic creep events or creeplets (Figure 5e & f). It is often difficult to identify the duration of surges because their anomalous slip rates converge slowly toward background velocities. Among the 207 instances of LPCAs we have identified, their displacements have a median amplitude of 1.64 mm, a median duration of 55 days and a median peak velocity of $6.7\text{x}10^{-8}$m/s, approximately 60 times greater than the fastest interseismic slip rates along the creeping section of the San Andreas Fault (Burford and Harsh, 1980; Lisowski and Prescott, 1981; Titus et al., 2006). Due to their long duration extending to substantial fraction of the annual cycle, LPCAs are intrinsically difficult to distinguish from natural seasonal signals. It is possible that some of these surges are related to seasonal changes in environmental conditions on the surface fault, or that additional LPCAs exist outside of the catalogue. The complete separation of months-long creep surges from long term seasonally-driven environmental changes accommodated by a constant elevated creep rate is a topic for future study.

5 Overview of accelerated creep processes in time and space

We now present a preliminary analysis of the temporal and spatial distribution of creep events in the catalogue. In the following sections, we analyse the occurrence of "creep events" as they were picked from the time series; specifically, we focus on episodic creep events (ECEs), long-period creep accelerations (LPCAs), and creeplets (CLTS). We did not include continuous creep (as it is not an event), we did not include afterslip (which often consists of ECEs), and we did not make a specific distinction for triggered slip. Possible triggering is described for each event in the catalogue with a link to the potentially triggering earthquake, but we did not separate it in the following plots. We next investigate the occurrence of ECEs, LPCAs, and creeplets over time, and we briefly investigate the characteristics of the instruments and slip events in each fault system in this study: California, Utah, Türkiye, Israel, and Pakistan.

5.1 Events through time

Figure 6a shows the cumulative count of slip events between 1980 and 2023, colour coded according to identified mechanism: ECEs in yellow, LPCAs in purple, and CLTS in blue. We find that the cumulative number of events in the catalogue increases by roughly 100 events per year with fluctuations as new instruments are installed or others abandoned. A notable change in the type of events that make up the cumulative total occurred in 2017, coinciding with the introduction of 1-minute sampling instruments (Figure 6b) that account for the rise in the detection of creeplets. The increase in more small events is a result of this instrumental improvement.

A major increase in the number of recorded creep events occurs as a result of earthquakes followed by afterslip. For example, the 100 days following the 2004 M 6.0 Parkfield earthquake saw 18 times more events than in the 100 days preceding it (Figure 7a). The 100 days after the event contain 4.8% of all of the events in the catalogue and account for 13.1% of all events recorded on all creepmeters from the beginning of the instrumental record to the occurrence of the Parkfield earthquake. Elsewhere on the San Andreas creeping segment, near San Juan Bautista, there is no such similar increase in the number of observed events (Figure 7b).

5.2 Events across space

The majority of the creep events we identify are from faults in California, where we identify 4919 aseismic slip events on data from 51 creepmeters at 44 sites in five distinct regions: Hayward (5 creepmeters, Figure 2a), San Juan Bautista (11 creepmeters at 7 sites, Figure 2b), Parkfield (15 creepmeters at 13 sites, Figure 2c), the Salton Trough (14 creepmeters, Figure 2d), and Ridgecrest (6 creepmeters at 5 sites, Figure 3a). The remaining 776 events come from the other global study regions. All regions are described in detail here.

5.2.1 Hayward, California

Five creepmeters have operated on the Hayward Fault since as early as 1994 and have used variable sampling rates from 1 second to 60 minutes. Most of these data were recorded at a sampling rate of 10 minutes. We identify 486 aseismic slip events, mostly episodic creep events, in this time interval (Figure 8a). The 15th and 85th percentiles of event amplitudes and durations are 0.16–0.88 mm and 2 to 23 days respectively (Figure 9a).

5.2.2 San Juan Bautista, California

Eleven creepmeters have operated in the San Juan Bautista region of Northern California at seven locations. Most of these instruments are installed on the San Andreas Fault, but one creepmeter (XSH1) is installed on the Calaveras Fault. Following repairs to XSH1 in 2020, this instrument was renamed from XSH1 to XSH2. Data from other locations have also been renamed following changes in instrumentation or measurement geometry, e.g., XHR1, 2 & 3 (Figure 2b). Most of the instruments in this region have operated since the 1980s or earlier, but two new sites (FCR1 & XSH1) were instrumented since 2020. The sampling rate of instruments prior to 2020 is mostly 10 minutes. However, six instruments (CWN1, FCR1, SJN1, XHR3, XMR1, XSH2) have been sampled at 1-minute intervals since 2018. In total we identify 1080 aseismic slip events in the San Juan Bautista region, mostly episodic creep events (Figure 8b). The 15th and 85th percentiles of event amplitudes and durations are 0.09–2.46 mm and 6.2 hours to 2.8 days respectively (Figure 9b).

5.2.3 Parkfield, California

In the Parkfield region, at the southern end of the central San Andreas Fault, California, we identify creep events on 15 creepmeters located at 13 sites (Figure 2c). Installation of these sites began soon after creep was detected in 1968. All sites north of Hwy 46 (i.e., C461) record at 10-minute sampling. Instrument C461, which replaced an older instrument following the 2004 M 6.0 Parkfield Earthquake, recorded at a 1 minute sampling rate. A total of 3079 aseismic slip events have been identified in the Parkfield region, mostly as episodic creep events (Figure 8c). The 15th and 85th percentiles of event amplitudes and durations are 0.13–1.29 mm and 9.8 hours to 3.7 days respectively (Figure 9c). This region accounts for $\approx$ 54% of all events we observe. Most of these events occur at XMM1, which alone accounts for $\approx$ 18% of all events in the catalogue, partly because the digital recording here has been continuous since the mid 1980s. Afterslip following the 2004 M 6.0 Parkfield earthquake also reduced the recurrence interval between creep events, temporarily increasing their abundance (Gittins and Hawthorne, 2022).

5.2.4 Salton Trough, California

Fourteen creepmeters have operated on the Southern San Andreas Fault, Imperial Fault, Superstition Hills Fault, San Jacinto Fault and minor faults north of the Laguna Salada Fault since the 1970's (Louie et al., 1985). In this work, we consider the archive of digital data from these instruments, which began around the year 2000. Sampling rates are mostly at 1-minute intervals with occasional periods of sampling as low as 60 minutes. In total, 230 aseismic slip events have been documented in the Salton Trough region with approximately equal numbers of creeplets and episodic creep events (Figure 8d). The 15th and 85th percentiles of event amplitudes and durations are 0.04–0.9 mm and 6.2 hours to 14.1 days respectively (Figure 9d). It should be noted that some events and event sequences in this region, particularly on the Superstition Hills Fault, occasionally exceed 20 mm and are amongst the largest recorded anywhere. Approximately 1 m of afterslip, dominantly in episodic slip events, occurred on the Superstition Hills Fault following a M-6.6 earthquake in 1987 (Bilham, 1989). In the past few decades, slip on the Superstition Hills Fault has typically occurred as large events (>1 cm) following prolonged intervals of quiescence, most recently 13 years (Vavra et al., 2024). Several of its aseismic slip events have been triggered by local or regional seismicity (Wei et al., 2015).

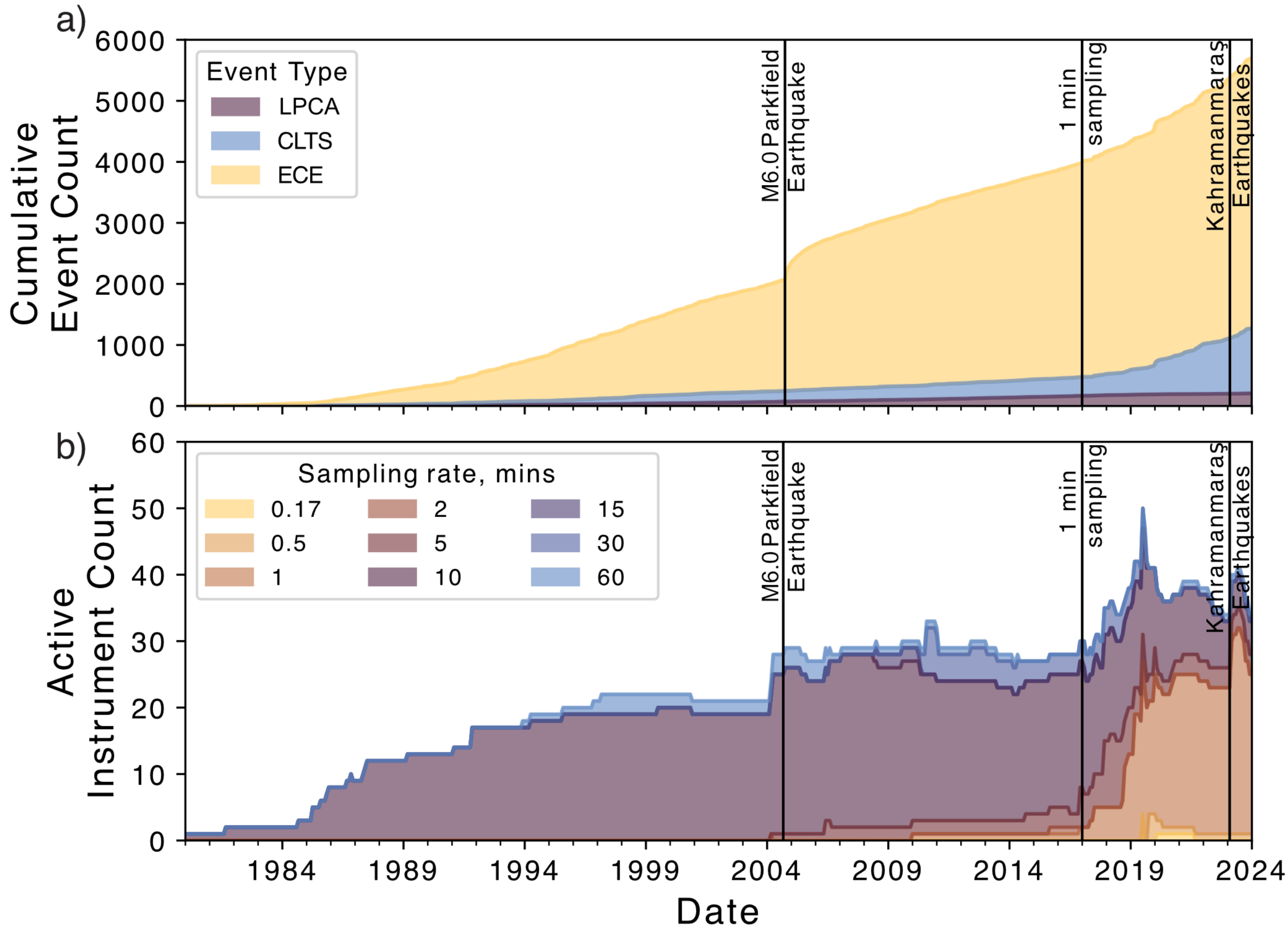

Figure 6 a) Cumulative aseismic slip events though time from 1980 to the end of 2023. b) Cumulative number of active creepmeters with time, colour coded by sampling rate in minutes. See supplementary tables S1 to S7 for complete creepmeter metadata.

5.2.5 Ridgecrest, California

Six creepmeters (Figure 2e) briefly operated on the Ridgecrest and Garlock Faults following the 2019 M 6.4 & 7.1 Ridgecrest earthquakes. Although they recorded several triggered slip events at the time of aftershocks, they recorded no afterslip or episodic slip events.

5.2.6 Utah

We identify 3 creeplets and 3 episodic creep events (Figure 8g) on a creepmeter installed on a normal fault in Canyonlands National Park (Figure 5f), Utah with a 30-minute sampling rate. This creepmeter was installed to measure displacements in a salt tectonics regime (Kravitz et al., 2020). The 15th and 85th percentiles of event amplitudes and durations are 0.07–0.27 mm and 2.1 days to 21.2 days respectively (Figure 10c).

5.2.7 North Anatolian Fault, Türkiye

Ten creepmeters have operated at various times between Izmit and the Ismetpasa region of the North Anatolian Fault starting in 2012 (Figure 4a/b). Sampling rates vary from 1 to 30 minutes. Within these data we have identified 422 aseismic slip events, with a higher relative number of creeplets compared to sites in California (Figure 8e). The 15th and 85th percentiles of event amplitudes and durations are 0.03–0.65 mm and 2.3 hours to 2.8 days respectively (Figure 10a). At Ismetpasa it is common for a multiple-slip-event sequence to cumulatively release up 1 cm of slip every few years.

5.2.8 East Anatolian Fault, Türkiye

Two creepmeters (Figure 4c) were installed on the East Anatolian Fault following the 2020 M 6.8 Sivrice earthquake, and a further 13 following the 2023 Kahramanmaraş sequence. These data are typically recorded at a sampling rate of 1 minute. Of the 328 aseismic slip events identified, 62.8% are creeplets (Figure 8f). The 15th and 85th percentiles of event amplitudes and durations are 0.03–0.21 mm and 2.5 hours to 1 day respectively (Figure 10b).

5.2.9 Israel

In early 2021, a dual axis creepmeter was installed across an oblique normal and left-lateral strike slip fault in the Dead Sea Fault system in Israel (Figure 3c) with a sampling rate of 20 seconds (Hamiel et al., 2025). Of the

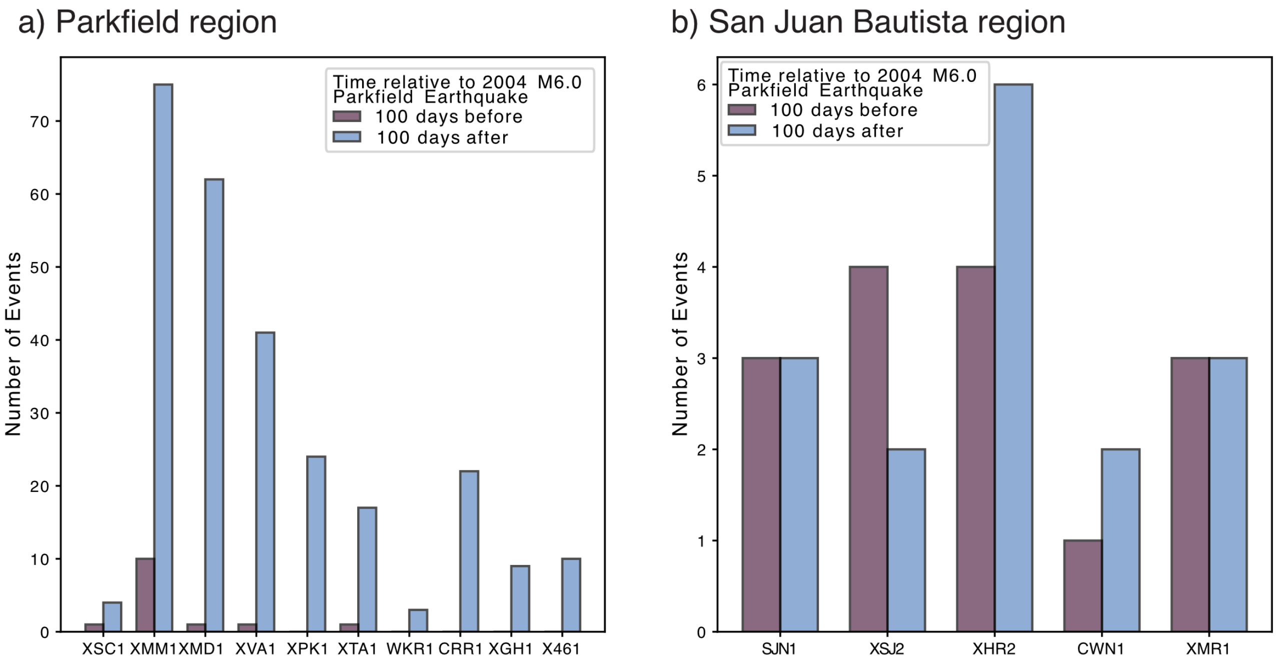

Figure 7 Number of events recorded in the 100 days before and after the 2004 M 6.0 Parkfield earthquake. a) Parkfield region, b) San Juan Bautista region. Creepmeters are ordered from left to right in North to South order.

16 aseismic slip events we identified, most are episodic creep events (Figure 8g). The 15th and 85th percentiles of event amplitudes and durations are 0.11–1.17 mm and 2.1 days to 22 days respectively (Figure 10c).

5.2.10 Pakistan

In 2019 several creepmeters were installed across the Chaman Fault in Pakistan (Figure 3d) with sampling rates of 10 minutes. During their almost-two-year operation, these instruments recorded four creep events consisting of two episodic creep events, one long-period creep acceleration and one creeplet (Figure 8g & 10c). The 15th and 85th percentiles of event amplitudes and durations are 0.19–2.8 mm and 1.6 days to 30.3 days respectively.

6 Discussion

The data presented here derive exclusively from surface creepmeters, which means they reflect the behaviour of the shallowest few meters of the fault zone as well as the fault at depth. One often overlooked issue in evaluating the time history of aseismic surface slip is that observed creep is expressed almost ubiquitously within a weathered sedimentary shear zone (i.e., dirt) that may differ from the rheology prevailing in the fault zone at depth. It has recently been recognized, for example, that the properties of this thin carapace of materials may arrest the propagation of ruptures to the surface (Brooks et al., 2017; Parker et al., 2021), and may arrest both coseismic slip and postseismic afterslip (Ambraseys, 1970; Bilham, 2005; Savage and Langbein, 2008). Nonetheless, the measurement of fault slip at the surface, and its transient accelerations over time and space, has value for understanding fault failure processes at and below the surface.

The creep event catalogue presented here allows us to investigate the global statistics of creep events and the relationships between parameters such as displacement and duration. As shown in Figures 9 and 10, the distribution of event displacement and duration vary across locations, even within regions of closely spaced creepmeters. Some creepmeter locations (e.g., XMR1, XMM1, INW1) appear to have bimodal distributions of displacements, a trend previously identified by Burford (1977), albeit for a smaller subset of events at one site (XMR1). The relationship between displacement and duration is also variable across sites, with some locations showing a positive linear relationship (e.g., Hayward instruments, Figure 9a) while others have more characteristic event durations despite having different displacements (e.g., XMM1, Figure 2c). Further analysis of these findings may reveal implications for the underlying physics governing aseismic creep, as has been inferred for subduction zone slow slip events (Ide et al., 2007).

One challenge in forming such scaling relationships is that the magnitude of creep events is generally unknown. Strain modeling shows that moment release in creep events is typically Mw«5, (Gittins and Hawthorne, 2024), but the magnitude of each individual event is relatively unconstrained. Few of the creep events in our event catalogue have been recorded by more than one instrument, as the spacing of creepmeters is typically much larger than the probable dimensions of a slipping patch in a creep event (Gittins and Hawthorne, 2022). More dense instrumentation, including borehole strain measurements, and space-geodetic analysis may be able to shed more light on the moment magnitude of

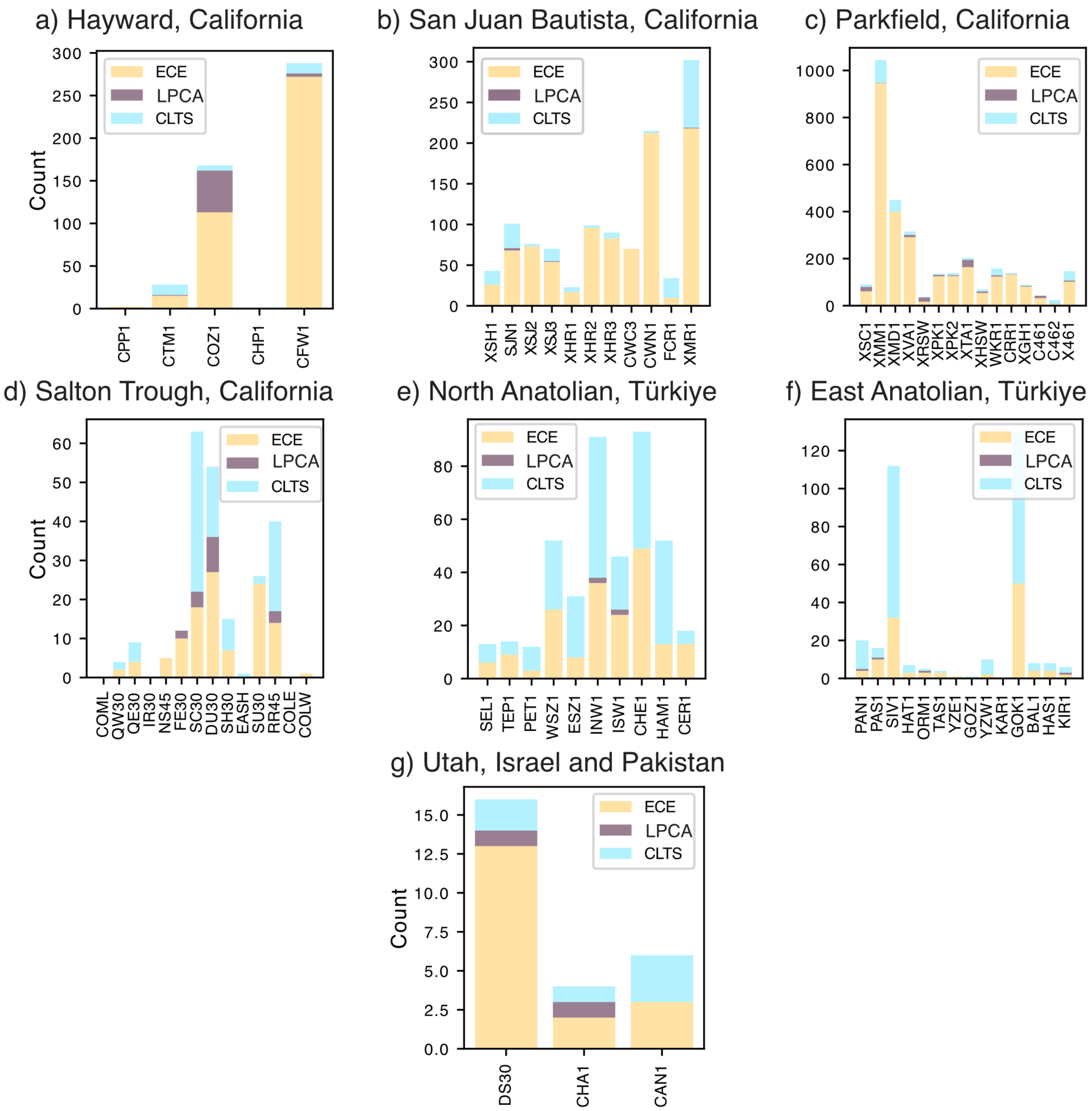

Figure 8 Number of Episodic creep Events (ECE), Long-period creep accelerations (LPCA) and Creeplets (CLTS) per creepmeter location in different locations: a) Hayward, b) San Juan Bautista, c) Parkfield, d) Salton Trough, e) North Anatolia, f) East Anatolia & g) Utah, Israel and Pakistan.

general creep events.

In this work, we present a new scheme for classifying discrete types of aseismic creep, identifying six phenomenological clusters that form a useful taxonomy for creepmeter observations. However, in reality, aseismic creep covers a more continuous spectrum of processes, meaning that faults may slip in hybrid modes or in more than one mode at once. For example, afterslip is often accommodated by a large sequence of ECEs, as was seen in the afterslip sequences of the 2004 M 6.0 Parkfield, 1987 M 6.6 Superstition Hills, 2019 M 6.4 & 7.1 Ridgecrest, and 2020 M 6.8 Sivrice earthquakes. Additionally, some triggered slip is distinct from typical ECEs by being more impulsive, but some triggered slip is essentially an ECE that occurred with a clock advance due to the dynamic triggering. We suggest that the categories presented here are a useful simplification of a broad spectrum; this taxonomy can allow future targeted study of various slip modes, but any categorization of such a spectrum of processes will necessarily be imperfect.

The catalogue we present here should also be interpreted with several important caveats. First, creepmeters with higher sampling rates can identify shorter and smaller events, leading to a change in the size distribution of events where sampling rates have been increased in recent years (Langbein et al., 2024). For example, a 50-minute creep event may present as only two samples in a dataset with 60 minute sampling, and therefore may not be recognized as a creep event until the sampling rate is increased. Higher sampling rates allow for more precise detection of creep events and ultimately a more accurate characterization of failure processes in the fault zone.

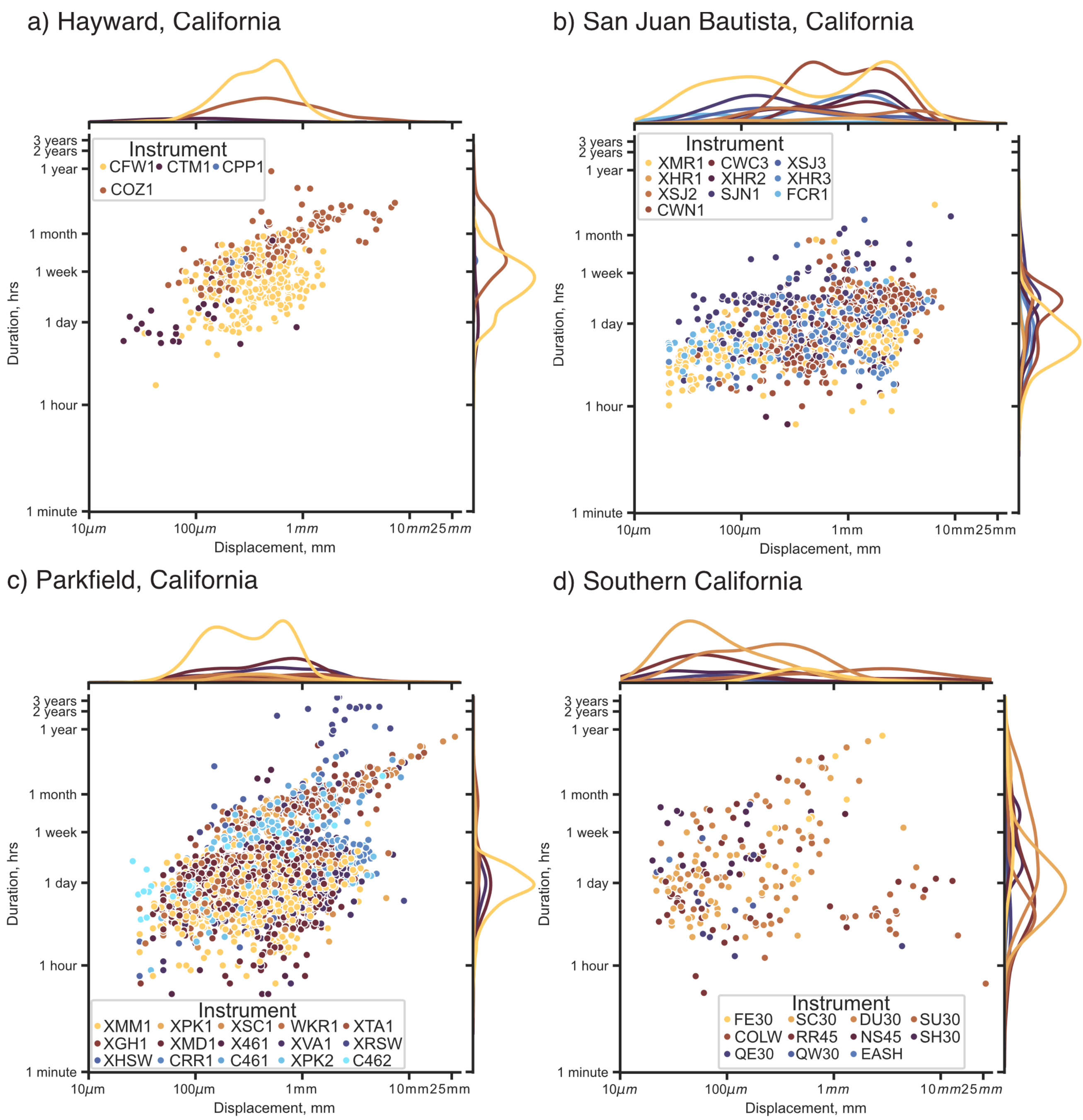

Figure 9 Displacement against duration plots for slip events for four regions in California. a) Hayward Fault events, b) San Juan Bautista region of the San Andreas and Calaveras Faults, c) Parkfield region of the San Andreas Fault, d) Salton Trough (Southern San Andreas Fault, Shoreline Faults, Superstition Hills Fault, Imperial Fault, and Laguna Salada Faults). The distributions on the top and right of each panel show the distribution of event sizes and durations for each creepmeter plotted.

Additionally, the specific criteria used for event-picking from the time series, and the duration of the events being picked, may change the details of the resulting catalogue. The distinction between LPCA and seasonal or background changes in creep rate is quite subtle, leading to certain events that may be picked by one person and not by another. The detection threshold also depends on the duration of the creep event in question, as shorter impulsive signals are much easier to identify than subtle long-period changes. Similar observational limitation issues also arise in other seismological studies of slow slip (Ide and Beroza, 2023). Quantifying creep-event detection thresholds as a function of event duration and station-specific noise quality would be a useful avenue of future work, eventually helping scientists use creep events to constrain the mechanical properties of the shallow fault zone and the shallow subsurface.

The dataset presented here could be used in a number of future studies and applications to better understand the mechanics of aseismic creep. The creep event catalogue produced here consists of a structured, labelled dataset with the timing, location, displacement, and duration of 5695 creep events. This dataset provides the large number of observations required to determine scaling relationships between parameters, including as

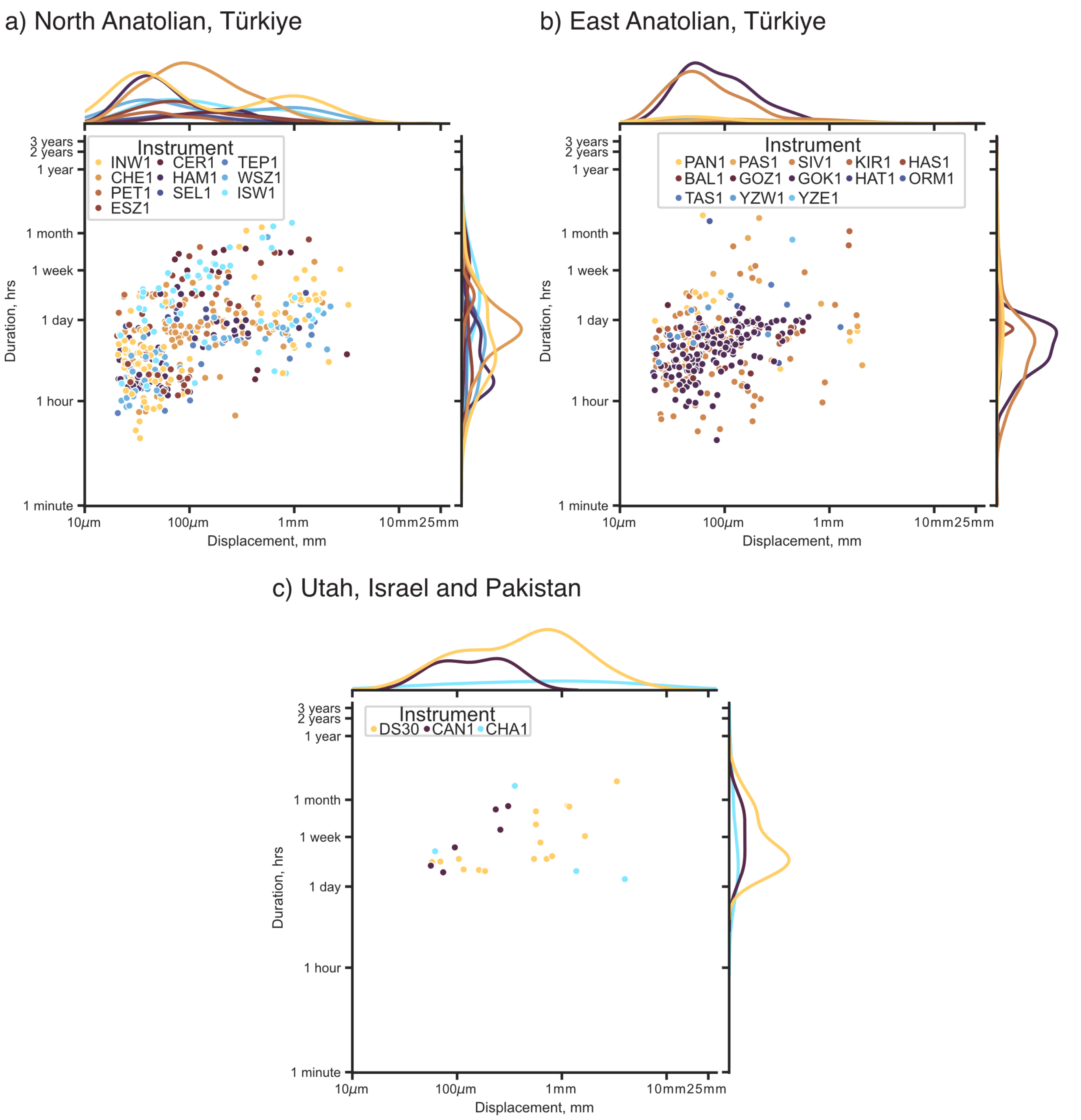

Figure 10 Displacement against duration plots for slip events in locations outside of California. a) North Anatolian Fault, Türkiye. b) East Anatolian Faults (East Anatolian Fault, Elbistan Fault & Sarıız Fault), Türkiye. c) Needles Fault Zone, Utah, Chaman Fault, Pakistan & Dead Sea Fault Zone, Israel. The distributions on the top and right of each panel show the distribution of event sizes and durations for each creepmeter plotted.

a function of space or time. We also anticipate that this dataset will be useful for future researchers wishing to conduct statistical seismology or as part of a training dataset for Machine Learning algorithms applied to raw creep data. In addition to providing the ability to conduct machine learning on surface rupturing creep events, we anticipate that our catalogue of aseismic slip events, when combined with raw creepmeter data, will also facilitate studies of the mechanics of aseismic slip on faults on which they have occurred and on faults elsewhere.

7 Summary and Conclusion

In this report, we summarise steps undertaken to compile a catalogue of surface rupturing aseismic slip events recorded on creepmeters on faults in California, Türkiye, Pakistan, and Israel between 1980-2023. The digital catalogue contains more than 5000 surface rupturing creep events with amplitude and duration information, permitting peak slip velocities and time constants to be derived in subsequent analysis. We distinguish and define six modes of aseismic slip in these data: steady creep, afterslip, triggered slip, long-period creep accelerations, episodic creep events and newly defined creeplets. We report which creepmeter locations record creep events of which types, highlighting first-order differences in aseismic behaviours between major creeping faults on Earth.

As part of our analysis we have released two datasets on Zenodo that can be used in conjunction with one another. The first is the catalogue described in this work (available from Gittins et al., 2025). The second dataset is newly updated and standardised creepmeter data for Türkiye and Southern California (available from Gittins and Bilham, 2025). These datasets provide the time series and creep event information required to analyse the time-evolution of thousands of creep events, investigate the rheology and potential interactions between creep events, and more, enabling new insights into the mechanics of shallow fault slip.

Acknowledgements

The U.S. Geological Survey National Earthquake Hazards Reduction Program is primarily responsible for the availability of much of the data we have examined in this study and we thank the numerous U.S. Geological Survey investigators who for the past five decades have maintained the creepmeter array in northern California. Caltech investigators were responsible for initiating creep measurements in southern California. Fatih Bulut and Asli Garagon have maintained the flow of data from the creepmeters in Izmit and Ismetpasa, on the North Anatolian Fault and Mehmet Kökūm was singularly responsible for the installation and maintenance of the Sivrice sensors on the East Anatolian Fault. Efe Turan Ayruk and his colleagues from Yildiz University have been instrumental in installing and acquiring data from the Kahramanmaras array. The Utah creepmeters were funded by NSF EAR1119173. The Chaman creepmeters were funded by NSF EAR 1561057. The Ridgecrest data were funded by NSF EAR1941558 and EAR 1650364 and by USGS 04HQAG0008. Data from the Sivrice and Kahramanmaras studies were made possible by NSF awards EAR 2019910, 13020909, 2318733 and EAR 2404835. Daniel Gittins was supported by the CIRES Visiting Fellows Program, funded by NOAA Cooperative Agreement: NA22OAR4320151. We thank Matt Wei, Sarah Titus, one anonymous reviewer, Josie Nevitt, and Curtis Baden who helped to improve the content and clarity of this manuscript. Any use of trade, firm or product names is for descriptive purposes only and does not imply endorsement by the U.S. Government.

Data and code availability

The catalogue of surface rupturing aseismic slip events is archived on Zenodo (Gittins et al., 2025). The raw California creepmeter data are archived by the United States Geological Survey (Langbein et al., 2024) and are available from https://earthquake.usgs.gov/monitoring/deformation/data/download.php. Fox Creek creepmeter data is archived on Zenodo and is available from Shaddox et al. (2022). Creepmeter data from Türkiye, Pakistan and Israel is available from (Gittins and Bilham, 2025). The surface rupturing aseismic slip detection software is archived on Zenodo and available from Gittins (2026).

Competing interests

The authors acknowledge that there are no conflicts of interest recorded.

References

Allen, C. R., Wyss, M., Brune, J. N., Grantz, A., and Wallace, R. E. Displacements on the Imperial, Superstition Hills and San Andreas Faults Triggered by the Borrego Mountain Earthquake. *U.S. Geol. Surv. Prof Pap.*, 787:87–104, 1972.

Ambraseys, N. Some characteristic features of the Anatolian fault zone. *Tectonophysics*, 9(2-3):143–165, 1970. doi: 10.1016/0040-1951(70)90014-4.

Barbour, A. J., Langbein, J. O., and Farghal, N. S. Earthquake Magnitudes from Dynamic Strain. *Bulletin of the Seismological Society of America*, 111(3):1325–1346, Mar. 2021. doi: 10.1785/0120200360.

Bilham, R. Surface slip subsequent to the 24 November 1987 Superstition Hills, California, earthquake monitored by digital creepmeters. *Bulletin of the Seismological Society of America*, 79(2):424–450, Apr. 1989. doi: 10.1785/BSSA0790020424.

Bilham, R. Coseismic Strain and the Transition to Surface Afterslip Recorded by Creepmeters near the 2004 Parkfield Epicenter. *Seismological Research Letters*, 76(1):49–57, Jan. 2005. doi: 10.1785/gssrl.76.1.49.

Bilham, R. and Castillo, B. The July 2019 Ridgecrest, California, Earthquake Sequence Recorded by Creepmeters: Negligible Epicentral Afterslip and Prolonged Triggered Slip at Teleseismic Distances. *Seismological Research Letters*, 91(2A):707–720, 2020. doi: 10.1785/0220190293.

Bilham, R. and Hough, S. E. Static and Dynamic Strain in the 1886 Charleston, South Carolina, Earthquake. *Bulletin of the Seismological Society of America*, 114(5):2687–2712, May 2024. doi: 10.1785/0120240025.

Bilham, R., Suszek, N., and Pinkney, S. California Creepmeters. *Seismological Research Letters*, 75(4):481–492, 2004. doi: 10.1785/gssrl.75.4.481.

Bilham, R., Ozener, H., Mencin, D., Dogru, A., Ergintav, S., Cakir, Z., Aytun, A., Aktug, B., Yilmaz, O., Johnson, W., and Mattioli, G. Surface creep on the North Anatolian Fault at Ismetpasa, Turkey, 1944–2016. *Journal of Geophysical Research: Solid Earth*, 121 (10):7409–7431, 2016. doi: 10.1002/2016JB013394.

Bilham, R., Ayruk, E. T., Turgut, M., Irguren, R., Kokum, M., Elhisso, A., Farimaz, I., and Dogan, U. Afterslip and Triggered Slip Following the 6 Feb 2023 Kahramanmaras Earthquake Sequence, East Anatolian Fault, Turkiye. In Ciner, A., Banerjee, S., Radwan, A., Hamimi, Z., Candeias, C., Meghraoui, M., and Laouar, R., editors, *Recent Research on Sedimentology, Stratigraphy, Paleontology, Tectonics, Geochemistry, Volcanology and Petroleum Geology*, pages 447–450. Springer Nature Switzerland, 2025. doi: 10.1007/978-3-031-87558-8_84.

Bodin, P., Bilham, R., Behr, J., Gomberg, J., and Hudnut, K. W. Slip triggered on southern California faults by the 1992 Joshua Tree, Landers, and big bear earthquakes. *Bulletin of the Seismological Society of America*, 84(3):806–816, June 1994. doi: 10.1785/BSSA0840030806.

Brooks, B. A., Minson, S. E., Glennie, C. L., Nevitt, J. M., Dawson, T., Rubin, R., Ericksen, T. L., Lockner, D., Hudnut, K., Langenheim, V., Lutz, A., Mareschal, M., Murray, J., Schwartz, D., and Zaccone, D. Buried shallow fault slip from the South Napa earthquake revealed by near-field geodesy. *Science Advances*, 3(7):e1700525, July 2017. doi: 10.1126/sciadv.1700525.

Bucknam, R. C. Documentation for alinement arrays, Motagua fault, Guatemala. Technical Report 78-880, U.S. Geological Survey, 1978. doi: 10.3133/ofr78880. Publication Title: Open-File Report.

Burford, R. O. Bimodal distribution of creep event amplitudes on the San Andreas fault, California. *Nature*, 268(5619):424–426, 1977. doi: 10.1038/268424a0.

Burford, R. O. and Harsh, P. W. Slip on the San Andreas fault in central California from alinement array surveys. *Bulletin of the Seismological Society of America*, 70(4):1233–1261, 1980. doi: 10.1785/BSSA0700041233.

Bürgmann, R. The geophysics, geology and mechanics of slow fault slip. *Earth and Planetary Science Letters*, 495:112–134, Aug. 2018. doi: 10.1016/j.epsl.2018.04.062.

Cakir, Z., Doğan, U., Akoğlu, A. M., Ergintav, S., Özarpacı, S., Özdemir, A., Nozadkhalil, T., Çakir, N., Zabcı, C., Erkoç, M. H., Basmenji, M., Köküm, M., and Bilham, R. Arrest of the Mw 6.8 January 24, 2020 Elaziğ (Turkey) earthquake by shallow fault creep. *Earth and Planetary Science Letters*, 608:118085, 2023. doi: 10.1016/j.epsl.2023.118085.

Donnellan, A., Parker, J., Hensley, S., Pierce, M., Wang, J., and Rundle, J. UAVSAR observations of triggered slip on the Imperial, Superstition Hills, and East Elmore Ranch Faults associated with the 2010 M 7.2 El Mayor-Cucapah earthquake. *Geochemistry, Geophysics, Geosystems*, 15(3):815–829, 2014. doi: 10.1002/2013GC005120.

Evans, K. F., Burford, R. O., and King, G. C. P. Propagating episodic creep and the aseismic slip behavior of the Calaveras Fault north of Hollister, California. *Journal of Geophysical Research: Solid Earth*, 86(B5):3721–3735, 1981. doi: 10.1029/JB086iB05p03721.

Freed, A. M. Afterslip (and only afterslip) following the 2004 Parkfield, California, earthquake. *Geophysical Research Letters*, 34 (6), 2007. doi: 10.1029/2006GL029155.

Gittins, D. and Hawthorne, J. Assessing creep event rheologies using their temporal evolution. *Seismica*, 5(1), May 2026. doi: 10.26443/seismica.v5i1.1890.

Gittins, D. B. dbgittins/Creep_event_detection_scripts: creepeventdetection, Jan. 2026. doi: 10.5281/zenodo.18433667.

Gittins, D. B. and Bilham, R. Standardised creepmeter time series data between 1980-2023 from Southern California, Türkiye, Pakistan and Israel, Sept. 2025. doi: 10.5281/zenodo.17087958.

Gittins, D. B. and Hawthorne, J. C. Are Creep Events Big? Estimations of Along-Strike Rupture Lengths. *Journal of Geophysical Research: Solid Earth*, 127(1):e2021JB023001, 2022. doi: 10.1029/2021JB023001.

Gittins, D. B. and Hawthorne, J. C. Scattered M3–4 Slip Bursts Within Creep Events on the San Andreas Fault. *Journal of Geophysical Research: Solid Earth*, 129(6):e2023JB028187, 2024. doi: 10.1029/2023JB028187.

Gittins, D. B., Materna, K., Crume, H., and Bilham, R. Digital catalogue of shallow aseismic slip bursts between 1980 – 2023 as recorded by creepmeters from the US, Türkiye, Pakistan and Israel, Oct. 2025. doi: 10.5281/zenodo.17064463.

Goulty, N. R. and Gilman, R. Repeated creep events on the San Andreas Fault near Parkfield, California, Recorded by a strainmeter array. *Journal of Geophysical Research*, 83(B11):5415, 1978. doi: 10.1029/JB083iB11p05415.

Hamiel, Y. and Piatibratova, O. Transient Behavior and Interplay Between Seismic and Aseismic Deformation Near the Tip of a Creeping Segment: Insights From the Northern Jordan Valley Segment of the Dead Sea Fault. *Geophysical Research Letters*, 50(3):e2022GL100584, 2023. doi: 10.1029/2022GL100584.

Hamiel, Y., Bilham, R., and Piatibratova, O. Characterizing Shallow Aseismic Deformation Along the Dead Sea Pull-Apart Basin Using Geodetic Observations. *Journal of Geophysical Research: Solid Earth*, 130(4):e2024JB030191, 2025. doi: 10.1029/2024JB030191.

Hudnut, K. W. and Clark, M. M. New slip along parts of the 1968 Coyote Creek fault rupture, California. *Bulletin of the Seismological Society of America*, 79(2):451–465, Apr. 1989. doi: 10.1785/BSSA0790020451.

Ide, S. and Beroza, G. C. Slow earthquake scaling reconsidered as a boundary between distinct modes of rupture propagation. *Proceedings of the National Academy of Sciences*, 120(32): e2222102120, Aug. 2023. doi: 10.1073/pnas.2222102120.

Ide, S., Beroza, G. C., Shelly, D. R., and Uchide, T. A scaling law for slow earthquakes. *Nature*, 447(7140):76–79, May 2007. doi: 10.1038/nature05780.

Johnson, K. M., Bürgmann, R., and Larson, K. Frictional Properties on the San Andreas Fault near Parkfield, California, Inferred from Models of Afterslip following the 2004 Earthquake. *Bulletin of the Seismological Society of America*, 96(4B):S321–S338, Sept. 2006. doi: 10.1785/0120050808.

King, C.-Y. A Shallow-Faulting Model. *Bulletin of the Seismological Society of America*, 62(2):551–559, 1972. doi: 10.1785/BSSA0620020551.

King, C.-Y., Nason, R. D., and Burford, R. O. Coseismic steps recorded on creep meters along the San Andreas Fault. *Journal of Geophysical Research (1896-1977)*, 82(11):1655–1662, 1977. doi: 10.1029/JB082i011p01655.

Kravitz, K., Mueller, K., Bilham, R. G., and Walton, M. Active Steady-State Creep on A Nontectonic Normal Fault in Southeast Utah: Implications for Strain Release in a Rapidly Deforming Salt System. *Geophysical Research Letters*, 47(11):e2020GL087081, 2020. doi: 10.1029/2020GL087081.

Langbein, J., Murray, J. R., and Snyder, H. A. Coseismic and Initial Postseismic Deformation from the 2004 Parkfield, California, Earthquake, Observed by Global Positioning System, Electronic Distance Meter, Creepmeters, and Borehole Strainmeters. *Bulletin of the Seismological Society of America*, 96(4B):S304–S320, 2006. doi: 10.1785/0120050823.

Langbein, J., Bilham, R. G., Snyder, H., and Ericksen, T. L. Summary of Creepmeter Data from 1980 to 2020—Measurements Spanning the Hayward, Calaveras, and San Andreas Faults in Northern and Central California. Open-File Report, USGS, Renton, Virginia, 2024. Series: Open-File Report DOI: 10.3133/ofr20241011.

Lienkaemper, J. J., Galehouse, J. S., and Simpson, R. W. Creep Response of the Hayward Fault to Stress Changes Caused by the Loma Prieta Earthquake. *Science*, 276(5321):2014–2016, June 1997. doi: 10.1126/science.276.5321.2014.

Lisowski, M. and Prescott, W. H. Short-range distance measurements along the San Andreas fault system in central California, 1975 to 1979. *Bulletin of the Seismological Society of America*, 71 (5):1607–1624, 1981. doi: 10.1785/BSSA0710051607.

Louie, J. N., Allen, C. R., Johnson, D. C., Haase, P. C., and Cohn, S. N. Fault slip in southern California. *Bulletin of the Seismological Society of America*, 75(3):811–833, June 1985. doi: 10.1785/BSSA0750030811.

Marone, C. J., Scholtz, C. H., and Bilham, R. On the mechanics of earthquake afterslip. *Journal of Geophysical Research: Solid Earth*, 96(B5):8441–8452, 1991. doi: 10.1029/91JB00275.

Materna, K., Bürgmann, R., Lindsay, D., Bilham, R., Herring, T., Crowell, B., and Szeliga, W. Shallow Slow Slip Events in the Imperial Valley With Along-Strike Propagation. *Geophysical Research Letters*, 51(12):e2023GL108089, 2024. doi: 10.1029/2023GL108089.

Nason, R. D., Philippsborn, F. R., and Yamashita, P. A. Catalog of creepmeter measurements in central California from 1968 to 1972. Technical Report 74-31, U.S. Geological Survey, 1974. doi: 10.3133/ofr7431. Publication Title: Open-File Report.

Parker, J., Donnellan, A., Bilham, R., Ludwig, L. G., Wang, J., Pierce, M., Mowery, N., and Jänecke, S. Buried Aseismic Slip and Off-Fault Deformation on the Southernmost San Andreas Fault Triggered by the 2010 El Mayor Cucapah Earthquake Revealed by UAVSAR. *Earth and Space Science*, 8(8):e2021EA001682, 2021. doi: 10.1029/2021EA001682.

Peng, Z. and Gomberg, J. An integrated perspective of the continuum between earthquakes and slow-slip phenomena. *Nature Geoscience*, 3(9):599–607, Sept. 2010. doi: 10.1038/ngeo940.

Perfettini, H. and Avouac, J.-P. Postseismic relaxation driven by brittle creep: A possible mechanism to reconcile geodetic measurements and the decay rate of aftershocks, application to the Chi-Chi earthquake, Taiwan. *Journal of Geophysical Research: Solid Earth*, 109(B2), 2004. doi: 10.1029/2003JB002488.

Ponti, D. J., Pickering, A. J., Blair, J. L., Rosa, C. M., Thomas, K., and Dawson, T. Digital Datasets Documenting Surface Fault Rupture and Ground Deformation Features Produced by the Ridgecrest M6.4 and M7.1 Earthquake Sequence of July 4 and 5, 2019, 2020. doi: 10.5066/P9BZ5IJ9.

Roeloffs, E. A. Creep rate changes at Parkfield, California 1966–1999: Seasonal, precipitation induced, and tectonic. *Journal of Geophysical Research: Solid Earth*, 106(B8):16525–16547, 2001. doi: 10.1029/2001JB000352.

Sacks, I. S., Suyehiro, S., Linde, A. T., and Snoke, J. A. Stress redistribution and slow earthquakes. *Tectonophysics*, 81(3):311–318, Jan. 1982. doi: 10.1016/0040-1951(82)90135-4.

Savage, J. C. and Langbein, J. Postearthquake relaxation after the 2004 M6 Parkfield, California, earthquake and rate-and-state friction. *Journal of Geophysical Research: Solid Earth*, 113(B10), 2008. doi: 10.1029/2008JB005723.

Schulz, S. S. Catalog of creepmeter measurements in California from 1966 through 1988. U.S. Geol. Surv. Open File Rep 89-650, U.S. Geological Survey, 1989. Series: Open-File Report.

Schulz, S. S., Burford, R. O., and Nason, R. D. Catalog of creepmeter measurements in central California from 1973 through 1975. Technical Report 77-31, U.S. Geological Survey„ 1976. doi: 10.3133/ofr7731. Publication Title: Open-File Report.

Schulz, S. S., Mavko, G. M., Burford, R. O., and Stuart, W. D. Long-term fault creep observations in central California. *Journal of Geophysical Research: Solid Earth*, 87(B8):6977–6982, 1982. doi: 10.1029/JB087iB08p06977.

Schulz, S. S., Burford, R. O., and Mavko, B. Influence of seismicity and rainfall on episodic creep on the San Andreas Fault System in central California. *Journal of Geophysical Research: Solid Earth*, 88(B9):7475–7484, 1983. doi: 10.1029/JB088iB09p07475.

Shaddox, H., Bilham, R., and Bürgmann, R. Fox Creek Ranch Creepmeter Data, Dec. 2022. doi: 10.5281/zenodo.7470791.

Smith, S. W. and Wyss, M. Displacement on the San Andreas Fault Subsequent to the 1966 Parkfield Earthquake. *Bulletin of the Seismological Society of America*, 58(6):1955–1973, 1968. doi: 10.1785/BSSA0580061955.

Steinbrugge, K. V., Zacher, E. G., Tocher, D., Whitten, C. A., and Claire, C. N. Creep on the San Andreas fault. *Bulletin of the Seismological Society of America*, 50(3):389–415, 1960. doi: 10.1785/BSSA0500030389.

Sylvester, A. G. 11 Near-Field Tectonic Geodesy. In *Active Tectonics: Impact on Society*. The National Academies Press, Washington, DC, 1986. doi: 10.17226/624.

Titus, S. J., DeMets, C., and Tikoff, B. Thirty-Five-Year Creep Rates for the Creeping Segment of the San Andreas Fault and the Effects of the 2004 Parkfield Earthquake: Constraints from Alignment Arrays, Continuous Global Positioning System, and Creepmeters. *Bulletin of the Seismological Society of America*, 96(4B): S250–S268, 2006. doi: 10.1785/0120050811.

Tocher, D. Fault creep in central California. *Eos, Transactions American Geophysical Union*, 50(5):385–385, 1969. doi: 10.1029/EO050i005p00385-01.

Tong, X. and Chen, S. Temporal and spatial variation of fault creep along the Xianshuihe fault from InSAR stacking. *Geophysical Journal International*, 241(2):1114–1131, May 2025. doi: 10.1093/gji/ggae310.

Tymofyeyeva, E., Fialko, Y., Jiang, J., Xu, X., Sandwell, D., Bilham, R., Rockwell, T. K., Blanton, C., Burkett, F., Gontz, A., and Moafipoor, S. Slow Slip Event On the Southern San Andreas Fault Triggered by the 2017 M_w 8.2 Chiapas (Mexico) Earthquake. *Journal of Geophysical Research: Solid Earth*, 124(9): 9956–9975, Sept. 2019. doi: 10.1029/2018JB016765.

USGS and CGS. Quaternary fault and fold database for the United States, 2020. https://www.usgs.gov/programs/earthquake-hazards/faults. Dataset.

Vavra, E. J., Fialko, Y., Rockwell, T., Bilham, R., Štěpančíková, P., Stemberk, J., Tábořík, P., and Stemberk, J. Characteristic Slow-Slip Events on the Superstition Hills Fault, Southern California. *Geophysical Research Letters*, 51(12):e2023GL107244, 2024. doi: 10.1029/2023GL107244.

Victor, P., Oncken, O., Sobiesiak, M., Kemter, M., Gonzalez, G., and Ziegenhagen, T. Dynamic triggering of shallow slip on forearc faults constrained by monitoring surface displacement with the IPOC Creepmeter Array. *Earth and Planetary Science Letters*, 502:57–73, Nov. 2018. doi: 10.1016/j.epsl.2018.08.046.

Wei, M., Liu, Y., Kaneko, Y., McGuire, J. J., and Bilham, R. Dynamic triggering of creep events in the Salton Trough, Southern California by regional M ≥ 5.4 earthquakes constrained by geodetic observations and numerical simulations. *Earth and Planetary Science Letters*, 427:1–10, Oct. 2015. doi: 10.1016/j.epsl.2015.06.044.

Wesson, R. L. Dynamics of fault creep. *Journal of Geophysical Research*, 93(B8):8929, 1988. doi: 10.1029/JB093iB08p08929.

Williams, P. L., McGill, S. F., Sieh, K. E., Allen, C. R., and Louie, J. N. Triggered slip along the San Andreas fault after the 8 July 1986 North Palm Springs earthquake. *Bulletin of the Seismological Society of America*, 78(3):1112–1122, June 1988. doi: 10.1785/BSSA0780031112.

Xu, X., Ward, L. A., Jiang, J., Smith-Konter, B., Tymofyeyeva, E., Lindsey, E. O., Sylvester, A. G., and Sandwell, D. T. Surface Creep Rate of the Southern San Andreas Fault Modulated by Stress Perturbations From Nearby Large Events. *Geophysical Research Letters*, 45(19):10,259–10,268, 2018. doi: 10.1029/2018GL080137.

Yamashita, P. and Burford, R. Catalog of preliminary results from an 18-Station creepmeter network along the San Andreas fault system in central California for the time interval June 1969 to June 1973. USGS Numbered Series 73-366, U.S. Geological Survey, Reston, VA, 1973. http://pubs.er.usgs.gov/publication/ofr73366.

Zelenin, E., Bachmanov, D., Garipova, S., Trifonov, V., and

Kozhurin, A. The Active Faults of Eurasia Database (AFEAD): the ontology and design behind the continental-scale dataset. *Earth System Science Data*, 14(10):4489–4503, Oct. 2022. doi: 10.5194/essd-14-4489-2022.